ANALYTICA CHIMICA ACTA 607 (2008) 168–175

available at www.sciencedirect.com

ScienceDirect

journal homepage: www.elsevier.com/locate/aca

Super-resolution and Raman chemical imaging: From multiple low resolution images to a high resolution image

Ludovic Duponchel[a,*], *Peyman Milanfar*[b], *Cyril Ruckebusch*[a], *Jean-Pierre Huvenne*[a]

[a] *Laboratoire de Spectrochimie Infrarouge et Raman, LASIR, CNRS UMR 8516, Bât. C5, Université des Sciences et Technologies de Lille, 59655 Villeneuve d'Ascq Cedex, France*

[b] *Multi-Dimensional Signal Processing Laboratory, Electrical Engineering Department, Baskin School of Engineering, University of California, 1156 High Street, Mailcode SOE2, Santa Cruz, CA 95064, USA*

ARTICLE INFO

Article history:
Received 15 October 2007
Received in revised form
28 November 2007
Accepted 3 December 2007
Published on line 8 December 2007

Keywords:
Super-resolution
Chemometrics
Raman spectroscopy
Imaging

ABSTRACT

Imaging in Raman spectroscopy is a valuable tool for analytical chemistry. Although molecular characterization at micron level is achieved for many applications, it usually fails producing chemical images of micron size samples as expected in chemical, environmental and biological analysis. The aim of the work is to introduce the potential of super-resolution in vibrational spectroscopic imaging. This original chemometrics approach uses several low resolution images of the same sample in order to retrieve a higher resolution chemical image. It is thus possible to overcome in a certain way some physical and instrumentals limitations. To illustrate the methodology, sub-micronic details of a Si/Au sample are retrieved from low resolution images with different super-resolution algorithms. The better results are obtained with Iterative L2/Bilateral Total Variation regularization method. The use of a regularization procedure gives also better results since its first property is to preserve edges during the reconstruction of the super-resolved image. This concept of chemical image data processing should open new analytical opportunities.

1. Introduction

For many imaging applications, obtaining high resolution images (HR) is a key step. An HR image, with its high pixel density, can present many details about the observed object. We have then a better vision of the reality and therefore better interpretations and knowledge. Since the 1970s, many imaging systems have been developed with different detector configurations as for example the well known charge-coupled device sensor (CCD). Such detectors have rapidly reached their limits of resolution, as people have sought more and more detailed images. The first way to increase the resolution of the devices is an instrumental one, whereby we could reduce the pixel size of the detectors. Nevertheless, pixel size reduction is balanced by a shot noise increase showing the existence of an optimally pixel size around 40 μm^2 even if lower pixel dimension is technologically possible. The second way to increase the resolution is to increase the chip size. Nevertheless, such devices are slower due to capacitance increase and moreover really costly.

The 1980s saw the beginnings of a growing area of signal processing called super-resolution (or superresolution). Super-resolution is defined by the use of image processing algorithms in order to overcome the limitations of optical systems [1–3]. The main advantage of such signal processing approach is that it costs less and the existing imaging systems can be still used. Moreover, due to physical limits it is sometimes the only way to increase resolution since no alternative instrumental

* *Corresponding author*. Tel.: +33 320436661; fax: +33 320436755.
E-mail address: ludovic.duponchel@univ-lille1.fr (L. Duponchel).
0003-2670/$ – see front matter © 2007 Elsevier B.V. All rights reserved.
doi:10.1016/j.aca.2007.12.004

setup may be available. The main idea of super-resolution is the fusion of several low-resolution images (LR) of the same object to obtain one higher-resolution image [4–6]. The first paper dealing with recovering HR image using multi-frames was written by Tsai and Huang [7]. It was shown that fusing under-sampled low resolution images with relative sub-pixel motion could give a super-resolution image with few or no aliasing effects. The great potential of the technique was illustrated in many fields such as video signal processing [8,9] medical imaging like functional MRI [10,11], positron emission tomography (PET) [12,13], X-ray imaging [14], forensic sciences [15,16], remote sensing [17,18], astronomy [19,20] or military applications [21,22].

Raman spectroscopic imaging is a powerful technique for visualizing the distribution of chemical compounds of complex samples based on the interaction of substance's molecular vibrations with laser light [23]. Due to the very high content of information contained in its spectrum, Raman spectroscopy has taken more and more importance in molecular imaging. With such far-field imaging spectroscopy, the resolution limit is first and foremost dictated by the photon wavelength due to diffraction limit and in a lesser manner by the detector area. For classical mapping procedures using visible photon for Raman scattering, 1 μm resolution images are usually considered optimal. Nevertheless this resolution limit is a real constraint, considering imaging spectroscopy of micron-sized samples such as in biology [24] or chemistry [25]. New chemometrics methods are now of great interest to overcome this drawback, while keeping our far-field Raman instruments.

To the best of our knowledge, this is the first paper dealing with such super-resolution concept applied to analytical chemistry and more precisely to molecular imaging spectroscopy like Raman scattering. The aim of the presented work is to show that fusing several 1 μm resolution images of the same sample acquired with sub-micron shifts can produce a HR image and in a certain way enable going beyond the physical limit to explore sub-micronic details.

2. Experimental

2.1. Materials

In order to test the proposed super-resolution methodology, sub-micronic patterns are produced on a sample surface. Moreover, the compound selected must have particularly good Raman scattering properties. The selection of a Si substrate is thus a perfect candidate. Electron beam lithography is used in this work to modify the Si surface [26]. It is carried out on the well known poly methyl methacrylate (PMMA) electron-sensitive resist materials. Solution of the resist is spin-coated onto a Si sample and baked to leave a hardened thin-film on the surface (around 500 nm, Fig. 1a). The beam system is then used to move a focused electron beam across the sample to selectively expose a pattern in the resist previously designed with computer software (Fig. 1b). Exposure of the positive tone resist to electrons causes fragmentation of the polymer chain into smaller molecular units (chain-scission). A developer solution is then used to selectively dissolve the fragmented polymer chains in the exposed areas of resist, whereas as the unexposed resist remains insoluble (Fig. 1c). The process leaves a patterned resist mask on the sample. This is transferred into the final sample using metal lift-off procedure. In a first step Au metal deposit by evaporation occurs (Fig. 1d). The remaining resist is then dissolved in a solvent lifting off the unwanted metal (Fig. 1e). Fig. 2b presents a SEM general view of the obtained Si sample with Au sub-micronic patterns. Fig. 2c corresponds to a sub-sample on which spectroscopic experiments and super-resolution were applied.

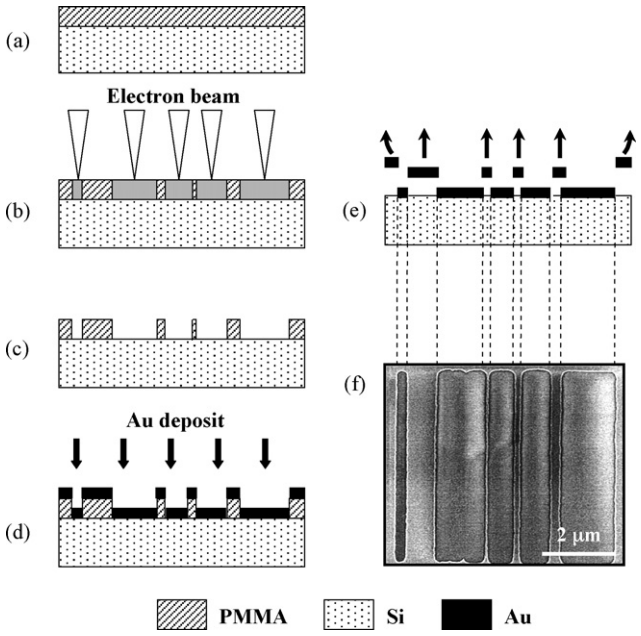

Fig. 1 – Sample preparation with electron lithography. Consecutive steps: PMMA polymer coated onto a Si sample (a); electron beam exposure (b); development phase (c); Au metal deposit by evaporation (d); Lift-off (e); SEM general view of the obtained Si sample with Au sub-micronic patterns (f).

2.2. Instrumentation

Raman microscopic measurements are carried out with a LabRAM confocal scanning spectrometer manufactured by Horiba Jobin Yvon (Fig. 3). The spectrometer is coupled confocally with an Olympus high-stability BX 40 microscope equipped with a ×100 objective (NA = 0.9). Before spectroscopic measurements, it is possible to have an optical view of the sample from a color camera. Raman backscattering is obtained with a 632.8 nm excitation wavelength supplied by a helium-neon laser (8 mW power). A liquid nitrogen-cooled CCD (Jobin-Yvon, 2048 × 512 pixels) is used for detection, allowing simultaneous spectral dispersion by a 1800 grooves mm^{-1} holographic grating over a 250–1300 cm^{-1} spectral range and 5 s spectrum acquisition time. The microscope stage is *XY*-motorized and computer controlled in order to assure the systematic moves over the sample. A 300 μm pinhole and a 150 μm slit are used. Like many other imaging systems, lateral resolution is determined by physical considerations and

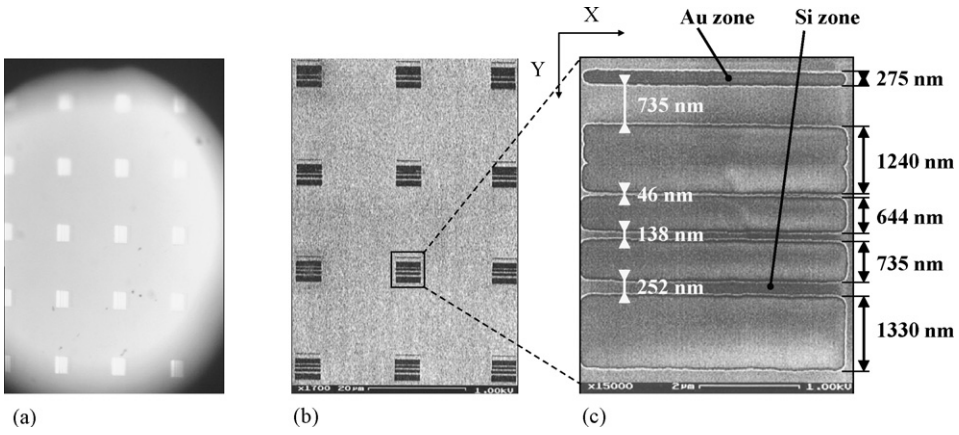

Fig. 2 – Si/Au sample presentation: optical view from visible microscope (a); SEM general view (b); the sub-sample with sub-micron details on which spectroscopic experiments and super-resolution were applied (c).

more precisely by the diffraction limit. It is then well admitted to consider the spatial extent of the laser focus around about 1 μm, a number that is derived from Eq. (1) below for an Airy disc of light:

$$x = \frac{1.22\lambda}{NA} \quad (1)$$

with x the distance between two nearby resolved points, λ the wavelength of the radiation used and NA the optical numerical aperture. This lateral resolution limit is thus considered to avoid diffraction effects and proposed unbiased cartography.

Taking into account the previous considerations, our spectroscopic experiments are defined as follows. For a first mapping experiment, acquisitions consisted in recording spectra with a 1 μm step in X and Y directions all over the sample. Thus, classical signal integration on a specific Si spectral contribution (515–525 cm^{-1}) produces the corresponding LR Si distribution image of size 9×7 pixels, each pixel corresponding in 1 μm^2 surface sample. Various sub-micron shifts (multiple of 0.1 μm) are applied from the first mapping grid to produce 49 other mapping experiments of the same sample and thus 49 other LR images defined as $\{\underline{Y}_k\}_{k=1}^{49}$. The 1 μm step spectral measurement over the sample is conserved for

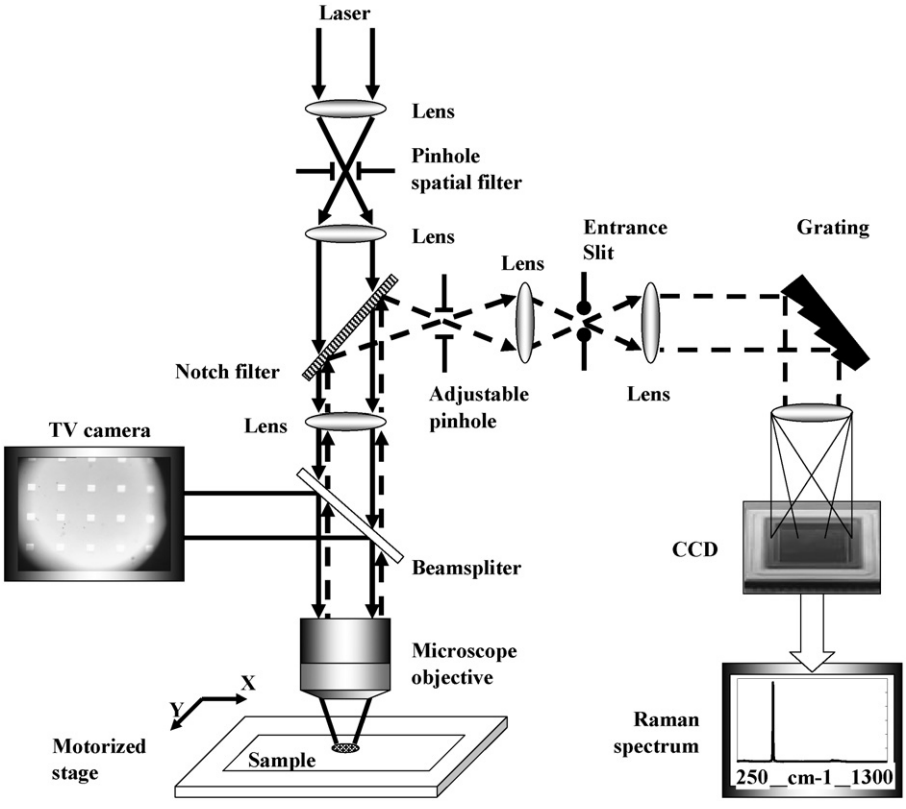

Fig. 3 – Raman microscopic device used for the super-resolution experiment.

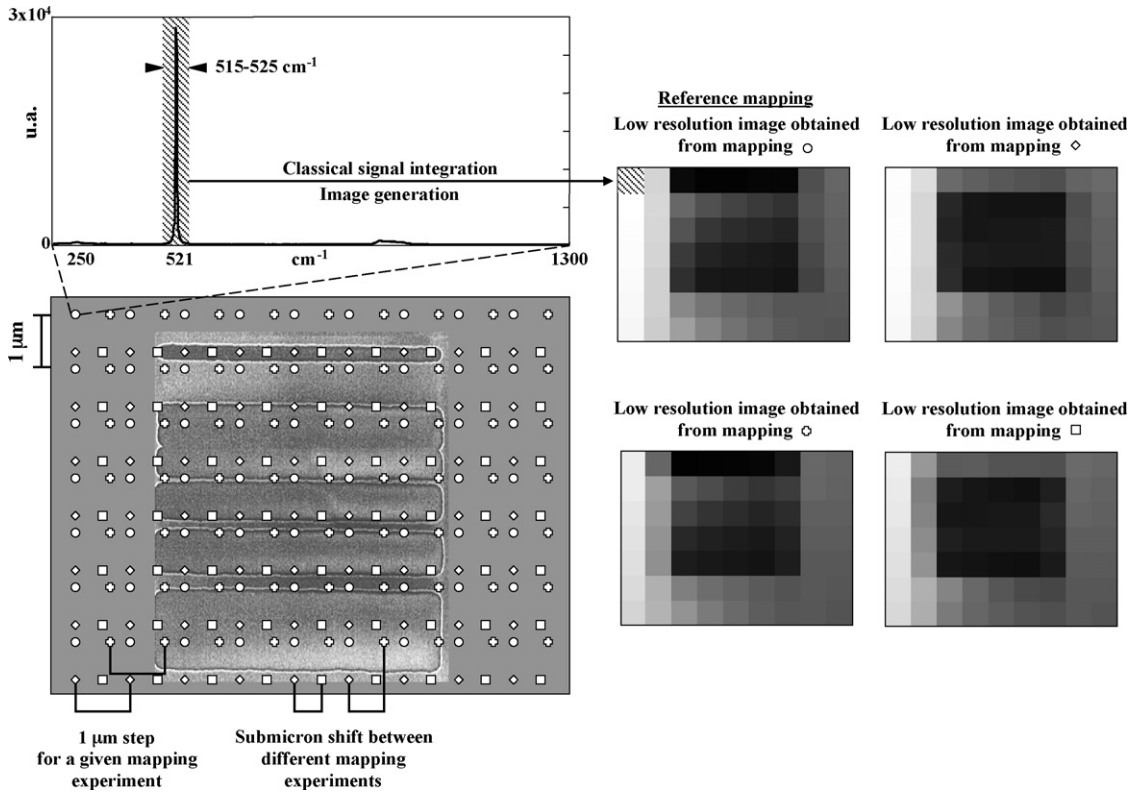

Fig. 4 – spectral analysis and mapping: spectral acquisition with a 1 µm step in X and Y directions all over the sample. Classical signal integration on a specific Si spectral contribution (515–525 cm^{-1}) to produce low resolution Si distribution images.

all mappings. The first mapping and three examples of submicron shift are presented in Fig. 4.

2.3. *Procedures*

The aim of this part is to propose a general but comprehensive analysis of the super-resolution concept. We first present the problem to be solved and then propose an analytical model to describe it. As in many papers dealing with image processing, images are represented column wise lexicographically ordered for matrix notation convenience.

Given are N measured images $\{\underline{Y}_k\}_{k=1}^{N}$, where each image is defined by $M \times M$ pixels and represented by the unfolded matrice $\underline{Y}_k$ of size $[M^2 \times 1]$. These LR images are different representations of a single HR ($L \times L$ pixels) represented by the unfolded matrice $\underline{X}$ of size $[L^2 \times 1]$, where $L > M$ for $1 \leq k \leq N$. In fact, it can be considered that each LR image measured is the result of a particular geometric warping (just translations in our microspectrometric case), linear space-invariant blurring, and uniform rational decimating performed on the ideal HR image $\underline{X}$. Additive Gaussian noise is also considered between low resolution images. It is thus possible to propose an analytical model (Eq. (2)), in order to express the steps described previously:

$$\underline{Y}_k = D_k H_k F_k \underline{X} + \underline{V}_k \quad (2)$$

The matrix F_k of size $[L^2 \times L^2]$ corresponds to the geometric warp operation between the $\underline{X}$ image and $\underline{Y}_k$. The matrix H_k of size $[L^2 \times L^2]$ is the blur matrix defined by the optical system's point spread function (PSF). [27] In other words, this function describes the response of an imaging system to a point source or point object. The matrix D_k of size $[M^2 \times L^2]$ corresponds to the decimation resulting in $\underline{Y}_k$. In other words, this step corresponds to the reduction of the number of observed pixels in the measured images. The additive Gaussian noise observed in the k-th measurement is described by the vectors $\{\underline{V}_k\}_{k=1}^{N}$ with zero mean. Fig. 5 provides a representation of the analytical model used in the super-resolution framework. As can be noticed, super-resolution is an inverse problem [28]. By definition, two problems are inverses of one another if the formulation of each involves all or part of the solution of the other. The aim of super-resolution is thus to estimate $\underline{X}$ based on the known images $\{\underline{Y}_k\}_{k=1}^{N}$. From the spectroscopist's point of view, it is a new approach to obtain a higher resolution image of a chemical sample from several low resolution images of it.

In order to use the proposed analytical model, we need to evaluate the availability of D_k, H_k and F_k matrices for all $k = 1, \ldots, N$. For many super-resolution applications, F_k have to be obtain by using motion estimation algorithms between low resolution images $\{\underline{Y}_k\}_{k=1}^{N}$ and one of the low resolution images (such as, say, $\underline{Y}_1$) chosen as a reference. Such methodologies are not necessary for our microspectrometric application

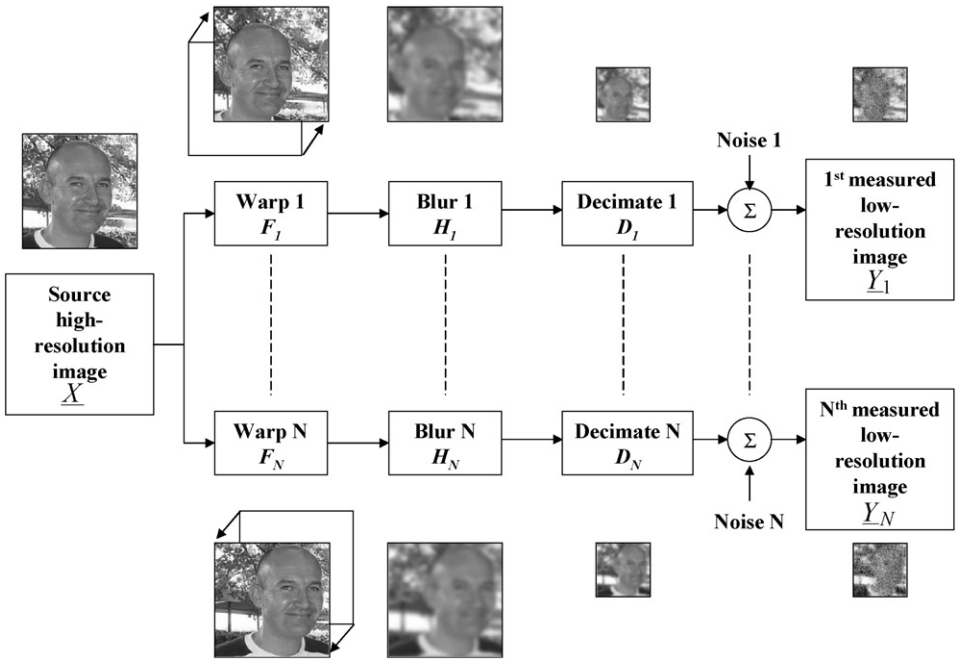

Fig. 5 – Representation of the analytical model used in super-resolution concept. Each low resolution image is a noisy, decimated, blurred and warped version of the original HR image.

since translational shifts between low resolution images are controlled by the motorized and computer-controlled stage, and therefore known quite accurately. Concerning H_k blur matrices, one can in general consider that all low resolution images are obtained with the same optical system and thus viewed through the same PSF that is to say $\forall k$, $H_k = H$. When possible, H is estimated with experiments or calculated from the optical pathlength. In our case, we observe that the super-resolution algorithm is robust to inexact knowledge of the H matrix, and thus it is possible to use a rough guess of it like a Gaussian filter. The matrix D_k is only dependant on the decimation ratio between the HR image and the LR measured image i.e. the ratio between the number of pixel in the LR image M^2 and the HR image L^2. The rule of thumb (Eq. (3)) gives an idea of the necessary low resolution image number N:

$$L^2 < NM^2 \tag{3}$$

The very important idea here is redundancy. That is to say, when possible, to measure a higher amount of data from the N LR images than the minimum amount necessary to build the HR image. If there are too few measured LR images, the resolution of Eq. (2) becomes an ill-posed problem which would find solutions only applying regularization procedures [28]. On the contrary, a high number of low resolution images will induce an underutilization of information but an improvement of the noise suppression. As typically in super-resolution problems, we consider here white noise:

$$E\{\underline{V}_k \underline{V}_k^{\mathrm{T}}\} = \sigma^2 I = W_k \tag{4}$$

Considering the analytical model (Eq. (2)) applied on the N LR images we have:

$$\begin{bmatrix} \underline{Y}_1 \\ \vdots \\ \underline{Y}_N \end{bmatrix} = \begin{bmatrix} D_1H_1F_1 \\ \vdots \\ D_NH_NF_N \end{bmatrix} \underline{X} + \begin{bmatrix} \underline{V}_1 \\ \vdots \\ \underline{V}_N \end{bmatrix} \tag{5}$$

It is now possible to retrieve the HR image $\underline{X}$ with classical restoration methods like Maximum-Likelihood estimation (ML) [37,29], Maximum *A Posteriori* estimation (MAP) [30–32], Projections Onto Convex Sets (POCS) [33,34] and others [35,36]. Using for example, the well known Maximum-Likelihood estimation procedure, estimation of $\underline{X}$ is obtained by the weighted least squares estimation of the form (Eq. (6)):

$$\hat{\underline{X}} = \underset{\underline{X}}{\mathrm{ArgMin}} \left\{ \sum_{k=1}^{N} [\underline{Y}_k - D_kH_kF_k\underline{X}]^{\mathrm{T}} W_k^{-1} [\underline{Y}_k - D_kH_kF_k\underline{X}] \right\} \tag{6}$$

Equating to zero the first derivative of (Eq. (6)) with respect to $\underline{X}$ we get:

$$\sum_{k=1}^{N} [D_kH_kF_k]^{\mathrm{T}} W_k^{-1} [\underline{Y}_k - D_kH_kF_k\underline{X}] = 0 \Rightarrow \mathbf{R}\hat{\underline{X}} = \mathbf{P} \tag{7}$$

$$\text{with} \quad \mathbf{R} = \sum_{k=1}^{N} F_k^T H_k^T D_k^T W_k^{-1} D_k H_k F_k \quad \text{and} \quad \mathbf{P} = \sum_{k=1}^{N} F_k^T H_k^T D_k^T W_k^{-1} \underline{Y}_k \tag{8}$$

Due the high dimension of the **R** matrix, solving Eq. (7) is tedious. Common iterative methods like steepest descent (SD) algorithm can be applied to obtain $\underset{\sim}{X}$ from **R** and **P** without inverting **R**. More details about this last step the regularization procedure can be found in Elad's paper [37]. Matlab v 7.1 computing environment (The Mathworks, MA, USA) and the freely available multi-dimensional signal processing (MDSP) toolbox [38] were used for all calculations reported below.

3. Results and discussion

The aim of super-resolution is to estimate a HR image based on the known LR images. The generic characteristic of such an inverse problem is that it is an ill-posed one. It effectively fails to satisfy one of the Hadamard's conditions [39]. This failure comes from either the characteristics of the optical system or the observed data. First, it is possible to observe the non-existence of a solution. Due to the presence of noise, the observed images can be inconsistent with *any* object at all. The result is that the system is noninvertible and the object cannot be estimated from the observations. Second, we can observe the nonuniqueness of the solution since we have only too few low resolution images. Since the number of unknowns exceeds the number of equations, we can say that insufficient equations exist to ensure the existence of a unique solution for our problem. Third, it is possible to observe a severe dependence of the solution on small changes in the data. Depending of the characteristics of the imaging system, the inverse problem can be very sensitive to perturbations of the data. In fact, such problem is invertible in theory but the inverse is unstable

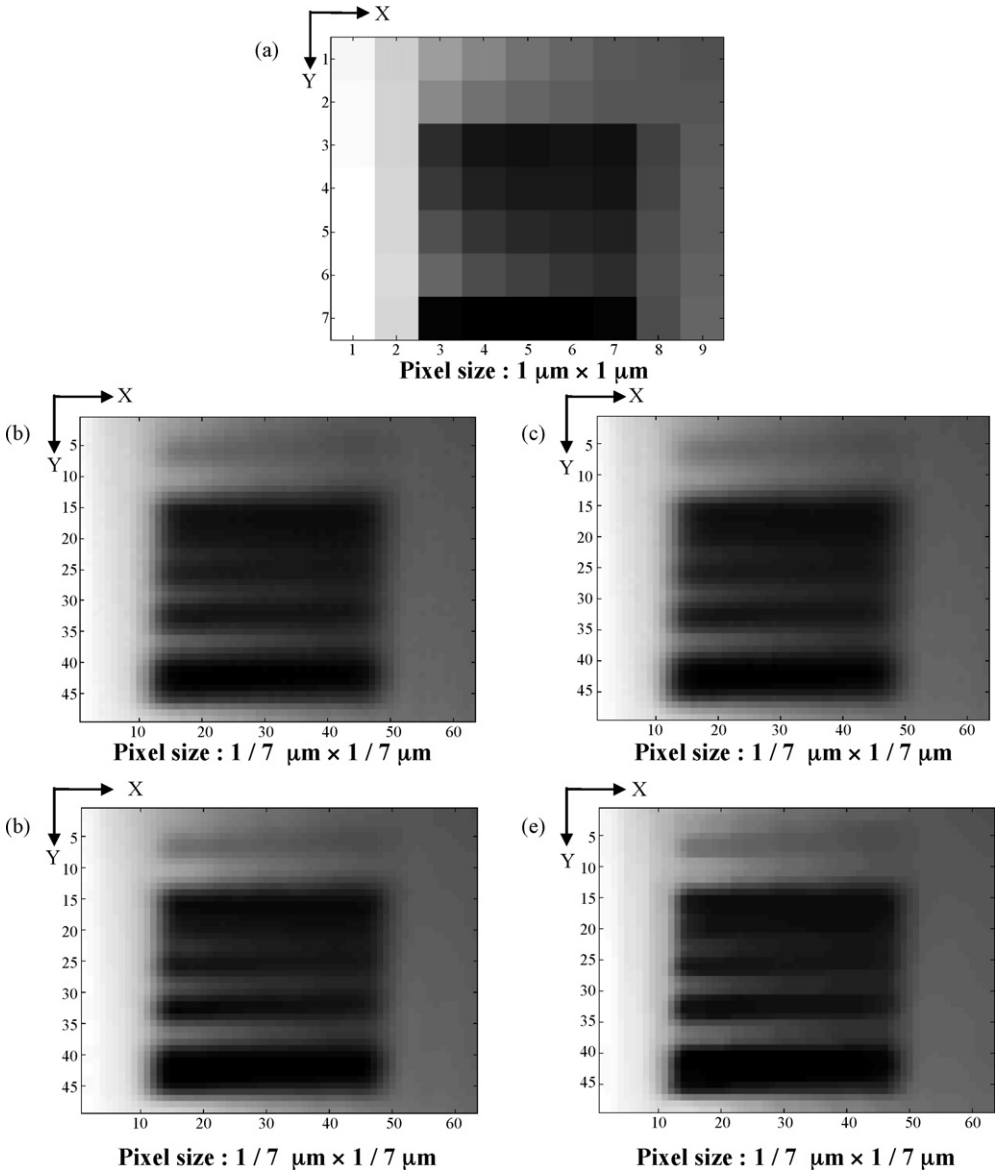

Fig. 6 – Super-resolution results. The reference LR image (a); HR image obtained with Shift-and-Add method (b); with Drizzle algorithm (c); with Iterative L2 and Tikhonov regularization (d); with Iterative L2 and Bilateral Total Variation regularization (e).

in practice i.e. small noise level in low resolution images leads to large spurious signal in the computed HR image.

In the presented work, we show that usual ill-posedness of the super-resolution problem can be overcome with regularization methods. Additional information is used to compensate for the information loss in LR images. This additional information is referred to prior information as it cannot be derived from observations. In general, the prior information is chosen to represent desired characteristics of the solution as for examples total energy, smoothness or positivity. Its role is thus to constrain and reduce the space of solutions which are compatible with the observed data. Fig. 6 presents the HR image obtained with various super-resolution methods. Compared to the reference low resolution image, we can notice a resolution enhancement factor of 7 with a new pixel surface equal to 1/49 μm^2. Sub-micron details around 260 nm can be observed on some super-resolved images like the Au and Si zones described on the SEM images. We can also observe that the Si signal (white color in all images) is really not constant in the X direction as we expected. This is an artefact explained by the choice of not using a laser depth control mechanism in Z direction during spectral acquisition in order to gain time. Nevertheless, without such a device, components from scattered light that were generated from above or below the desired position (ideally the first 300 nm from surface) within the sample were also detected and thus had degraded the quality of spectral data and observed LR images. Proposed super-resolution images were obtained with the Shift-and-Add method [29], Drizzle method [40] Iterative L2/Tikhonov regularization method [37] and Iterative L2/Bilateral Total Variation regularization method. [41] Shift-and-Add and Drizzle methods are the simplest techniques for inversion, and present the worst results with less sub-micronic details and rather low contrasts. We also observe a higher smoothing effect on their super-resolution results. In comparison, the two other regularized iterative L2 methods extract more features. Nevertheless, the better results are obtained with Iterative L2/Bilateral Total Variation regularization method compared to Iterative L2/Tikhonov regularization method. Tikhonov regularization is one of the most referenced methods [42]. The general principle of such method is to limit or penalize the total energy of the image. The consequence is thus to converge to a super-resolved image with no sharp edges. Same smoothing behaviours have been observed in Bayesian MAP framework [43] not so far from Tikhonov regularization concept. As described in Farsiu's paper [1] Bilateral Total Variation regularization method gives better results since its first property is to preserve edges during the reconstruction of the super-resolved image. Nevertheless, super-resolution results between Bilateral Total Variation and Tikhonov were not so different in our case certainly because of a low signal to noise ratio in LR images we used.

Results demonstrate the necessity of a regularization procedure. It is in fact the only way to find a stable solution to super-resolution problems. Regularization also improved the rate of convergence of super-resolution methods and sometimes removed artefacts even if it was not seen for our application. We can say that regularization was a good way to compensate the missing measurement information in the LR images.

4. Conclusion

This work presents the first attempt to use super-resolution methodology applied to vibrational imaging spectroscopy. Its particular characteristic is that it involves computational post-processing of the observed LR images. This is extremely attractive since the performance of existing Raman micro spectrometers can be enhanced without any requirements to modify the classical instrumentation. This first feasibility study showed very interesting results concerning the use of Bilateral Total Variation regularization method in order to retrieve sub-micron details of samples. Future works will be focused on the study of factors affecting the performance of multi-frame super-resolution restoration. It will correspond to an optimization of the super-resolution process with the principal idea of finding even better resolution enhancement.

From an instrumental point of view, it is really important to know if a better sub-micron motion precision between LR images is necessary. New instrumental setups like a piezo-driven nano-translation XY stage and an optical table with vibration control will be considered. The effect of signal to noise ratio on spectra and thus on LR images will be studied following some work of Robinson and Milanfar [44]. The number of necessary LR images should be estimated as the influence of relative motions between them.

From a chemometrics point of view, it will be essential to verify that the observation model accurately represents the processes which produce the observed LR images. If not, a better model specific to vibrational spectroscopy will permit to retrieve a better super-resolved image. The determination of the best regularization method for such spectroscopic applications is yet another step.

As final words, considering two decades of research and applications of the signal processing community, the future of super-resolution methods in spectroscopy appears promising because of a possible general extension to many imaging spectroscopic devices. We are convinced it will provide new trends in analytical chemistry.

REFERENCES

[1] S. Farsiu, M.D. Robinson, M. Elad, P. Milanfar, IEEE Trans. Image Process. 13 (2004) 1327.
[2] S. Farsiu, D. Robinson, M. Elad, P. Milanfar, Int. J. Imag. Syst. Technol. 14 (2004) 47.
[3] M.K. Ng, N.K. Bose, IEEE Signal Process. Mag. 20 (2003) 62.
[4] S.C. Park, H.K. Park, M.G. Kang, IEEE Signal Process. Mag. 20 (2003) 21.
[5] M.M. Hadhoud, F. Abd El-Samie, S.E. El-Khamy, Proceedings of the IEEE Conference on Fourth Workshop Photon. and Appl, 2004, p. 2.
[6] N. Nguyen, P. Milanfar, G. Golub, IEEE Trans. Image Process. 10 (2001) 573.
[7] R.Y. Tsai, T.S. Huang, Advances in Computer Vision and Image Processing, JAI Press, 1984.
[8] K.V. Suresh, G. Mahesh Kumar, A.N. Rajagopalan, IEEE Trans. Intell. Transp. Syst. 8 (2007) 321.
[9] Z. Xu, X. Zhu, J. Electron. 24 (2007) 363.
[10] R.R. Peeters, P. Kornprobst, M. Nikolova, S. Sunaert, T. Vieville, G. Malandain, R. Deriche, O. Faugeras, P. Van Hecke, Int. J. Imag. Syst. Technol. 14 (2004) 131.

[11] S. Peled, Y. Yeshurun, Magn. Reson. Med. 45 (2001) 29.
[12] A. Kennedy, O. Israel, A. Frenke, R. Bar-Shalom, H. Azhari, Int. J. Biomed. Imag. (2007) 46846.
[13] J.A. Kennedy, O. Israel, A. Frenkel, R. Bar-Shalom, H. Azhari, IEEE Trans. Med. Imag. 25 (2006) 137.
[14] P. Bernhardt, M. Lendl, F. Deinzer, Pediatr. Radiol. 36 (2006) 212.
[15] Z. Geradts, J. Bijhold, J. Forensic Sci. Soc. 41 (2001) 159.
[16] J. Fryer, K. McIntosh, Photogramm. Eng. Remote Sens. 67 (2001) 741.
[17] M.T. Merino, J. Núñez, IEEE Trans. Geosci. Remote Sens. 45 (2007) 1446.
[18] J. Núñez, M. Merino, Proceedings of the 25th Asian Conference on Remote Sensing, 2004, p. 262.
[19] K.G. Puschmann, F. Kneer, Astron. Astrophys. 436 (2005) 373.
[20] J.L. Starck, E. Pantin, F. Murtagh, Publ. Astron. Soc. Pac. 114 (2002) 1051.
[21] J.H. Cha, E. Jacobs, Proc. SPIE—Int. Soc. Opt. Eng. 5784 (2005) 107.
[22] S.S. Young, R.G. Driggers, Appl. Opt. 45 (2006) 5073.
[23] I.R. Lewis, H.G. Edwards, Handbook of Raman Spectroscopy: From the Research Laboratory to the Process Line, Marcel Dekker, Inc. Edition, New York, 2001.
[24] N.M. Sijtsema, S.D. Wouters, C.J. De Grauw, C. Otto, J. Greve, Appl. Spectrosc. 52 (1998) 348.
[25] L. Markwort, B. Kip, J. Appl. Polym. Sci. 61 (1996) 231.
[26] M. Gentili, C. Giovannella, S. Selci, Nanolithography: A Borderland Between STM, EB, IB and X-Ray Lithographies (NATO Science Series E:), Springer ed., 1994.
[27] T. Williams, The Optical Transfer Function of Imaging Systems, Taylor & Francis ed., 1998.
[28] J.B. Keller, Am. Math. Mon. 83 (1976) 107.
[29] M. Elad, Y. Hel-Or, IEEE Trans. Image Process. 10 (2001) 1187.
[30] R.R. Schultz, R.L. Stevenson, IEEE Trans. Image Process. 5 (1996) 996.
[31] R.C. Hardie, K.J. Barnard, E.E. Armstrong, IEEE Trans. Image Process. 6 (1997) 1621.
[32] R.R. Schultz, R.L. Stevenson, IEEE Trans. Image Process. 3 (1994) 233.
[33] H. Stark, P. Oskoui, J. Opt. Soc. Am. A, Opt. Image Sci. Vis. 6 (1989) 1715.
[34] A.J. Patti, M.I. Sezan, A.M. Tekalp, IEEE Trans. Image Process. 6 (1997) 1064.
[35] S. Chaudhuri, Super-Resolution Imaging, Springer ed., 2001.
[36] D. Capel, Image Mosaicing and Super-resolution, Springer ed., 2004.
[37] M. Elad, A. Feuer, IEEE Trans. Image Process. 6 (1997) 1646.
[38] http://www.soe.ucsc.edu/~milanfar/SR-Software.htm.
[39] J. Hadamard, Lectures on the Cauchy Problem in Linear Partial Differential Equations, Yale University Press, New Haven, CT, 1923.
[40] A.S. Fruchter, R.N. Hook, Publ. Astron. Soc. Pac. 114 (2002) 144.
[41] A. Zomet, A. Rav-Acha, S. Peleg, Proceedings of the IEEE Computer Society Conference on Computer Vision and Pattern Recognition 1, 2001, p. 1645.
[42] A.N. Tikhonov, V.A. Arsenin, Solutions of Ill-Posed Problems, Winston, Washington, DC, 1977.
[43] C. Bouman, K. Sauer, IEEE Trans. Image Process. 2 (1993) 296.
[44] D. Robinson, P. Milanfar, IEEE Trans. Image Process. 15 (2006) 1413.